

光学学报

完美涡旋光束在大气湍流传输中的螺旋相位谱分析

李思瑶, 丁洲林, 侯春雨, 王玮君, 马佳欣, 于永吉*

长春理工大学物理学院吉林省固体激光技术与应用重点实验室, 吉林长春 130022

摘要 基于Rytov近似,理论推导了完美涡旋光束(PVB)经过大气湍流水平信道后的螺旋相位谱解析表达式,研究了大气湍流中光束波长、半环宽、发射处轨道角动量(OAM)模态、光束半径、近地面折射率结构常数以及湍流系数对OAM模态探测概率和串扰概率的影响。结果表明:随着发射处OAM模态、传输距离、光束半径、近地面折射率结构常数以及湍流系数的增加,经大气湍流传输后的探测概率下降;随着光束波长的增加,经大气湍流传输后的探测概率增加。此外,PVB在近场的探测概率几乎不随发射处OAM模态变化,而当光束传输到远场时,探测概率随发射处OAM模态变化明显,这是因为PVB传输到远场变成类贝塞尔光束,其光束半径随发射处OAM模态变化明显。

关键词 大气光学; 完美涡旋光束; 轨道角动量; 湍流大气; 螺旋相位谱

中图分类号 O436 文献标志码 A

DOI: 10.3788/AOS230857

1 引言

涡旋光束是一种携带轨道角动量(OAM)的光束^[1]。常见的涡旋光束有拉盖尔-高斯光束^[2-3]、贝塞尔光束^[4-6]等。2013年,Ostrovsky等^[7]首次提出完美涡旋光束(PVB)的概念,该光束具有光束半径不随OAM模态增大而增大的特性,即不同阶次的PVB半径均相同。PVB在操控微粒、量子信息编码以及自由空间光通信等领域有较大的应用价值^[8-11]。涡旋光束的不同OAM模态相互正交,可用来拓展光通信系统的信道容量,涡旋光束的OAM维度也可用来对信号编码^[12],由于OAM模态的模式数不受限制(可取任意整数),理论上可使一个码元承载无穷大的信息量。然而,涡旋光束在大气中传输时因受到大气湍流的影响而产生畸变,大气湍流使其光强分布变得不均匀,螺旋相位产生畸变,导致螺旋谱扩展,引起不同模态的涡旋光束发生串扰,从而降低通信系统的信噪比,导致实际应用中的通信质量下降^[13-15]。

2020年,Yang等^[16]研究了PVB在大气湍流中传输的保束特性,通过调节PVB的半径和环宽,显著提升了PVB在不同大气湍流环境中传输时的保束特性。2011年,黎芳等^[17]研究了Rytov近似下拉盖尔-高斯光束在弱湍流大气中的螺旋谱(即OAM谱)特性。2015

年,Zhu等^[18]研究了non-Kolmogorov湍流对大气链路中超几何高斯光束螺旋谱的影响,确定了混合高斯光束OAM模态的探测概率和串扰概率。2017年,Liu等^[19]研究了non-Kolmogorov湍流下拉盖尔-高斯光束在斜程大气传输中的螺旋谱特性。2021年,Wang等^[20]研究了non-Kolmogorov湍流大气中高阶椭圆高斯涡旋光束的螺旋谱。目前,PVB在大气湍流传输中的螺旋相位谱特性研究鲜有报道。

本文基于Rytov近似理论,以PVB为模型,推导了PVB在接收孔径处的螺旋相位谱解析表达式,建立了PVB OAM模态的探测概率和串扰概率模型,分析了PVB在湍流大气传输中不同参数的影响以及光强分布特性。

2 理论模型

PVB在源平面($z=0$)中的光场分布^[21]表示为

$$E(r_0, \theta_0, z=0) = A_0 \exp\left(-\frac{r_0^2}{\omega_0^2}\right) I_m\left(\frac{2r_0 r_0}{\omega_0^2}\right) \exp(im\theta_0), \quad (1)$$

式中: A_0 为恒定振幅; m 为PVB发射平面处的OAM模态; I_m 为修正的第一类贝塞尔函数; r_0 为光束半径; ω_0 为PVB的半环宽;光束亮环的宽度为 $2\omega_0$ 。

PVB在自由空间中的光场分布^[21]为

$$E(r, \theta, z) = A_0 \frac{\omega_0}{\omega} (-1)^m \exp(i\psi + im\theta + ikz) \exp\left[\frac{ik}{2R'}(r^2 + r_r^2)\right] \times \exp\left\{-\frac{1}{\omega^2} \left[r^2 - \left(\frac{r_r z}{z_r}\right)^2\right]\right\} I_m\left[\frac{2rr_r \exp(i\psi)}{\omega_0 \omega}\right], \quad (2)$$

收稿日期: 2023-04-21; 修回日期: 2023-05-29; 录用日期: 2023-05-31; 网络首发日期: 2023-06-28

基金项目: 吉林省自然科学基金(20210101154JC)

通信作者: *yyjcust@163.com

式中: ω 为光束在 z 处的半径; R' 为曲率半径; ψ 为高斯光束的Gouy相移; k 为波数。其中,光束参数 ω 、 R' 和 ψ 与半环宽和瑞利距离 $z_r = k\omega_0^2/2$ 有关,表达式为

$$\begin{cases} \omega = \omega_0 \sqrt{1 + (z/z_r)^2} \\ R' = z + z_r^2/z \\ \psi = \arctan(z/z_r) \end{cases} \quad (3)$$

根据Rytov近似,弱湍流区^[22]的PVB在大气湍流中传输的复振幅可表示为

$$U(r, \theta, z) = E(r, \theta, z) \exp[\psi_0(r, \theta, z)], \quad (4)$$

式中: $\exp[\psi_0(r, \theta, z)]$ 为大气湍流对光束的复相位扰动。

$$\begin{aligned} \langle |a_l(r, z)|^2 \rangle &= \frac{1}{2\pi} \int_0^{2\pi} \int_0^{2\pi} \langle U(r, \theta, z) U^*(r, \theta', z) \rangle \exp[-il(\theta - \theta')] d\theta d\theta' = \\ &\quad \frac{1}{2\pi} \int_0^{2\pi} \int_0^{2\pi} U(r, \theta, z) U^*(r, \theta', z) \times \langle \exp[\psi_0(r, \theta, z) + \psi_0^*(r, \theta', z)] \rangle \exp[-il(\theta - \theta')] d\theta d\theta' \end{aligned} \quad (7)$$

式中: $\langle \cdot \rangle$ 表示对湍流的系综平均;上标*表示复共轭。

采用non-Kolmogorov概率谱描述大气湍流对PVB OAM模态的影响,non-Kolmogorov概率谱假定内尺度 $l_0 = 0$ 和外尺度 $L = \infty$,忽略内外尺度的效应。利用波结构函数的二次近似^[19],得到

$$\begin{aligned} \langle \exp[\psi_0(r, \theta, z) + \psi_0^*(r, \theta', z)] \rangle &\approx \\ &\exp\left[-\frac{2r^2 - 2r^2 \cos(\theta - \theta')}{\rho_0^2}\right], \end{aligned} \quad (8)$$

式中: ρ_0 为在non-Kolmogorov湍流中传输的球面波空间相干半径^[23]。

$$\begin{aligned} \langle |a_l(r, z)|^2 \rangle &= \frac{A_0^2 \omega_0^2 (-1)^{2m}}{2\pi \omega^2} \exp\left\{-2\left[r^2 - \left(\frac{r_r z}{z_r}\right)^2\right]\right\} \left| I_m \frac{2rr_r \exp(i\psi)}{\omega \omega_0} \right|^2 \times \\ &\exp\left(\frac{-2r^2}{\rho_0^2}\right) \int_0^{2\pi} \int_0^{2\pi} \exp[-i(l-m)(\theta - \theta') + \frac{2r^2 \cos(\theta' - \theta)}{\rho_0^2}] d\theta' d\theta \end{aligned} \quad (10)$$

积分公式为

$$\int_0^{2\pi} \exp[-in\varphi_1 + \eta \cos(\varphi_1 - \varphi_2)] d\varphi_1 = 2\pi \exp(-in\varphi_2) I_n(\eta), \quad (11)$$

式中: $I_n(\eta)$ 为第一类 n 阶修正贝塞尔函数。

将式(11)代入式(10),可以简化计算并得到PVB的OAM模态概率密度的解析表达式:

$$\langle |a_l(r, z)|^2 \rangle = \frac{2\pi A_0^2 \omega_0^2 (-1)^{2m}}{\omega^2} \exp\left\{-2\left[r^2 - \left(\frac{r_r z}{z_r}\right)^2\right]\right\} \left| I_m \frac{2rr_r \exp(i\psi)}{\omega \omega_0} \right|^2 \times \exp\left(\frac{-2r^2}{\rho_0^2}\right) I_{m-l}\left(\frac{2r^2}{\rho_0^2}\right). \quad (12)$$

当发射处OAM模态为 m 时,可以将接收处OAM模态为 l 的螺旋谐波能量定义为

$$C_l = \int_0^R \langle |a_l(r, z)|^2 \rangle r dr, \quad (13)$$

式中: R 为光束的接收孔径。

将式(12)代入式(13),得到PVB在大气湍流中的螺旋谱解析解表达式

$$C_l = \frac{2\pi A_0^2 \omega_0^2 (-1)^{2m}}{\omega^2} \int_0^R \exp\left\{-2\left[r^2 - \left(\frac{r_r z}{z_r}\right)^2\right]\right\} \left| I_l \frac{2rr_r \exp(i\psi)}{\omega \omega_0} \right|^2 \times \exp\left(-\frac{2r^2}{\rho_0^2}\right) I_{m-l}\left(\frac{2r^2}{\rho_0^2}\right) r dr, \quad (14)$$

式中: I_{m-l} 为 $m-l$ 阶第一类修正贝塞尔函数。

将螺旋相位谱 P_l 定义为 OAM 模态为 l 的螺旋谐波能量与光束总能量的比值, 表示为

$$P_l = \frac{C_l}{\sum_{q=-\infty}^{\infty} C_q}, \quad (15)$$

式中: $\sum_{q=-\infty}^{\infty} C_q$ 为各级螺旋谐波的总能量。当 $l=m$, 即

发射平面处的 OAM 模态为 m 时, P_m 表示在接收平面处 OAM 模态为 m 的探测概率; 当 $l=m+\Delta m$, 即发射平面处的 OAM 模态为 $m+\Delta m$ 时, $P_{\Delta m}$ 表示在接收平面处 OAM 模态为 $m+\Delta m$ 的串扰概率, 其中 Δm 为 OAM 模态差值 ($\Delta m \neq 0$)。

3 数值分析

利用第 2 节推导的 PVB 螺旋谱解析解, 分析光束的波长、发射处 OAM 模态、光束半径、半环宽、近

地面折射率结构常数以及湍流系数对螺旋谱的影响。除非另有说明, 本文采用的初始参数为: 振幅 $A_0=0.1$, 湍流系数 $\alpha=3.4$, 波长 $\lambda=1064 \text{ nm}$, 半环宽 $\omega_0=0.02 \text{ m}$, 光束半径 $r_r=0.08 \text{ m}$, 接收孔径 $R=0.2 \text{ m}$, 发射平面处的 OAM 模态 $m=1$, 近地面折射率结构常数 $C_n^2=1 \times 10^{-15} \text{ m}^{-2/3}$ 。

对自由空间光通信中光源波长 λ 的选择是提高通信效率的关键。波长 λ 对 PVB 探测概率 P_m 以及串扰概率 $P_{\Delta m}$ 的影响如图 1 所示。从图 1(a)可以看出: 随着传输距离的增加, 探测概率曲线呈下降趋势, 螺旋谱的扩展程度逐渐增大; 当传输距离一定时, 随波长 λ 的增加, 探测概率逐渐增大, 螺旋谱的扩展程度逐渐减小。从图 1(b)可以看出, 不同波长 λ 对应的串扰概率 $P_{\Delta m}$ 随着传输距离的增加而增大, 并且波长 λ 越小, 串扰概率 $P_{\Delta m}$ 越大, 其原因是: 随着传输距离的增加或者波长的减小, 空间相干半径 ρ_0 减小, 大气湍流引起的模态串扰变得严重, 螺旋谱的扩展增大。

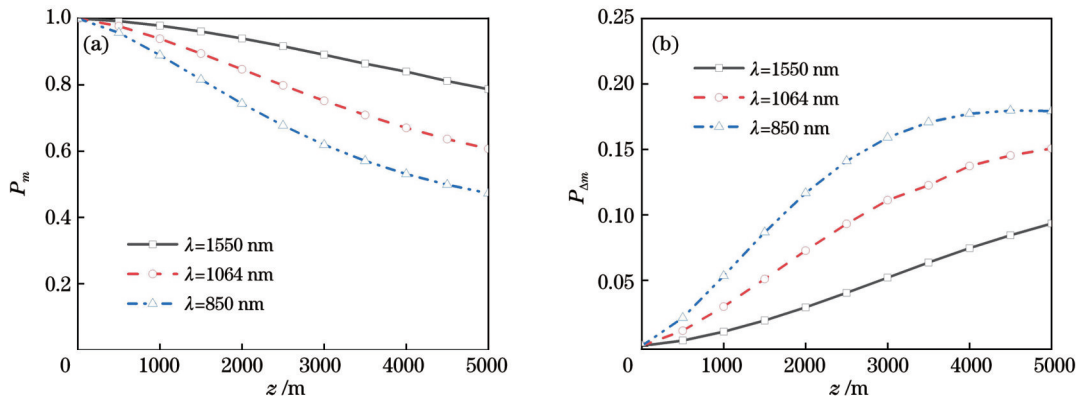


图 1 不同波长下探测概率 P_m 和串扰概率 $P_{\Delta m}$ 随传输距离的变化。(a) 探测概率 P_m ; (b) 串扰概率 $P_{\Delta m}$

Fig. 1 Variations of detection probability P_m and crosstalk probability $P_{\Delta m}$ with transmission distance at different wavelengths.
(a) Detection probability P_m ; (b) crosstalk probability $P_{\Delta m}$

半环宽 ω_0 对 PVB 探测概率 P_m 以及串扰概率 $P_{\Delta m}$ 的影响如图 2 所示, 其中 $\omega_0=0.02, 0.03, 0.05 \text{ m}$ 都在 PVB 半环宽的正常范围内。从图 2(a)可以看出, 尽管

探测概率曲线随传输距离呈下降趋势, 螺旋谱的扩展程度增大, 但半环宽 ω_0 的变化对探测概率 P_m 的影响很小。从图 2(b)可以看出, 当 $\Delta m=1$ 时, 不同半环宽

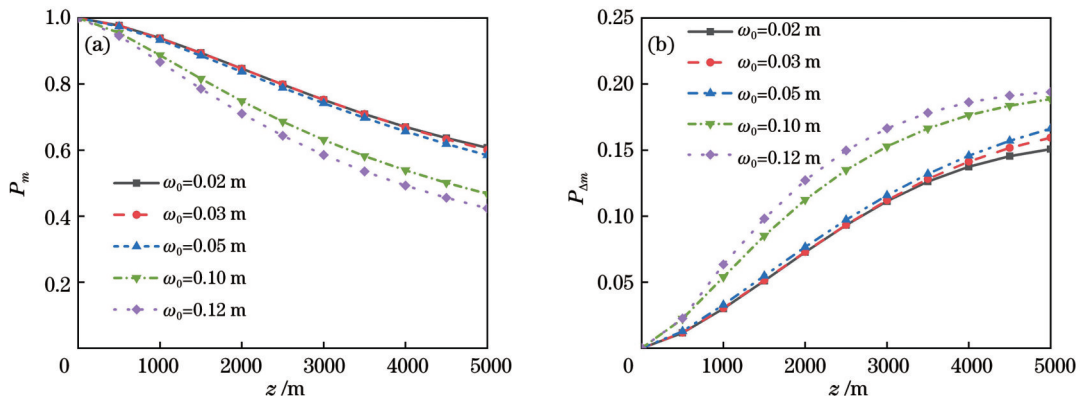


图 2 不同半环宽下探测概率 P_m 和串扰概率 $P_{\Delta m}$ 随传输距离的变化。(a) 探测概率 P_m ; (b) 串扰概率 $P_{\Delta m}$

Fig. 2 Variations of detection probability P_m and crosstalk probability $P_{\Delta m}$ with transmission distance under different half-ring widths.
(a) Detection probability P_m ; (b) crosstalk probability $P_{\Delta m}$

ω_0 对应的串扰概率 $P_{\Delta m}$ 相差很小。简而言之, 正常范围内, 半环宽 ω_0 的改变对 PVB 螺旋谱的扩展无大影响。

此外,PVB 的光束半径与光束宽度之比越大, 其越接近理想 PVB^[24]。当半环宽较大时, 光束不再呈现完美涡旋。当半环宽数值增加至 0.1 m(非 PVB)时, 其探测概率随传输距离增加呈明显下降趋势, 串扰概率呈增加趋势。因此,PVB 的光束半径与宽度之比越大, 其越接近 PVB 模型, 传输过程中目标 OAM 模态的探测概率越大, 湍流导致的模态串扰越小。

图 3 所示为发射处 OAM 模态 m 对 PVB 探测概率 P_m 以及串扰概率 $P_{\Delta m}$ 的影响。从图 3(a)可以看出: 随着发射处 OAM 模态 m 的增加, 探测概率曲线下降; 在传输至 2000 m 之前, 不同发射处 OAM 模态 m 对应的探测概率曲线几乎重合; 在传输至 2000 m 之后, 不同

初始发射处 OAM 模态 m 对应的探测概率曲线的差值明显增大。一个合理的解释是 PVB 在近场中具有光束半径不随发射处 OAM 模态 m 改变而变化的特性, 而在远场, 光束变成类贝塞尔光束, 光斑大小随发射处 OAM 模态 m 变化明显。图 4 所示为 PVB 在湍流大气中传输的数值仿真结果。根据 non-Kolmogorov 概率谱的 non-Kolmogorov 湍流三维功率谱^[25], 采用多层次相位屏法将 50 次模拟计算得到的结果进行平均, 计算出 PVB 湍流大气传输的平均光强。从图 3(b)可以看出, 在 $\Delta m = 1$ 条件下, 当传输距离超过 2000 m 时, 发射处 OAM 模态 m 越大, 串扰概率 $P_{\Delta m}$ 越大, 并且串扰概率 $P_{\Delta m}$ 主要发生在两个相邻 OAM 模态之间。因此, 当近地面折射率结构常数为 $C_n^2 = 1 \times 10^{-15} \text{ m}^{-3/2}$ 时, $\Delta m = 2, 3, 4, \dots$ 在接收器平面处的串扰可以忽略不计。

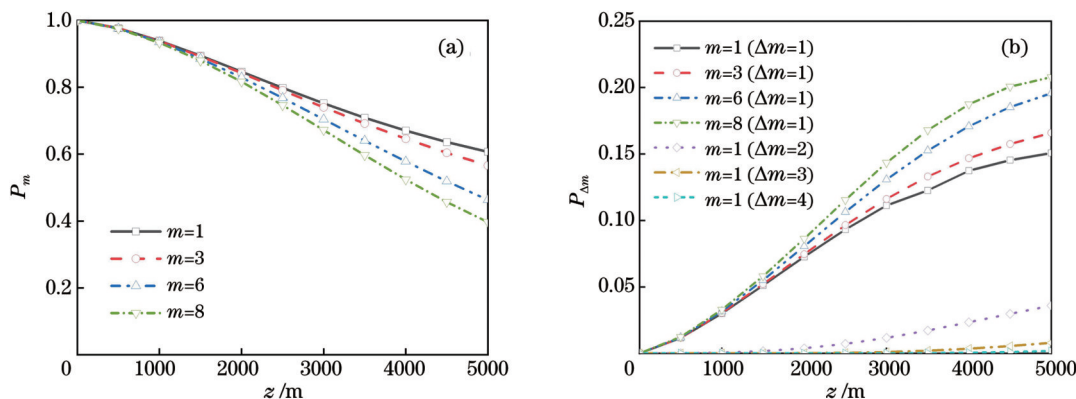


图 3 不同发射 OAM 模态下探测概率 P_m 和串扰概率 $P_{\Delta m}$ 随传输距离的变化。(a) 探测概率 P_m ; (b) 串扰概率 $P_{\Delta m}$
Fig. 3 Variations of detection probability P_m and crosstalk probability $P_{\Delta m}$ with transmission distance under different OAM modes.
(a) Detection probability P_m ; (b) crosstalk probability $P_{\Delta m}$

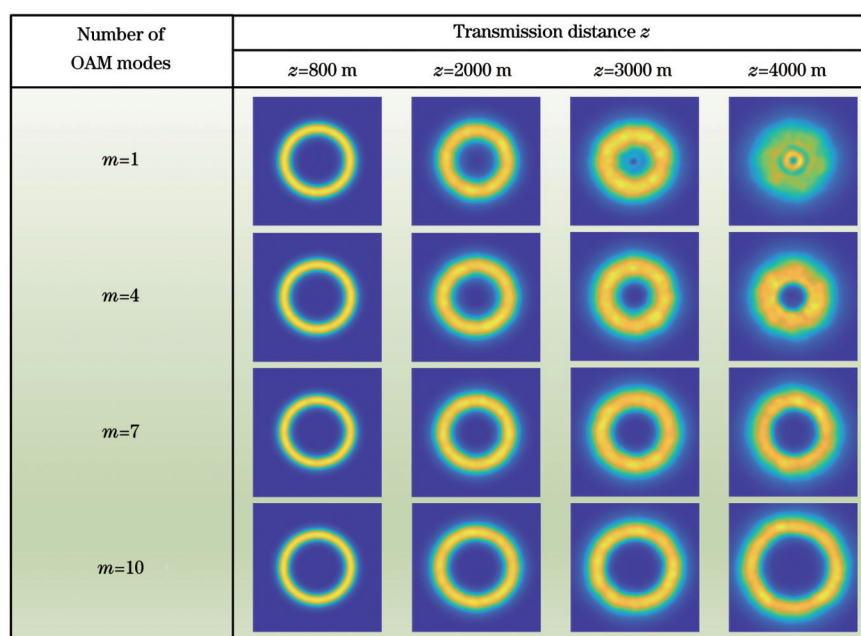


图 4 $m=1, 4, 7, 10$ 时, PVB 在大气湍流传输中光强随传输距离 z 的变化
Fig. 4 Variations of light intensity of PVB in atmospheric turbulence transmission with transmission distance z when $m=1, 4, 7$, and 10

PVB的探测概率 P_m 与串扰概率 $P_{\Delta m}$ 受近地面折射率结构常数 C_n^2 的影响如图5所示。从图5(a)不难看出,探测概率曲线在 $C_n^2=1\times 10^{-16}\text{m}^{-2/3}$ 下几乎保持不变,在 $C_n^2=1\times 10^{-15}\text{m}^{-2/3}$ 下随传输距离的增加逐渐下降,在 $C_n^2=5\times 10^{-15}\text{m}^{-2/3}$ 和 $C_n^2=1\times 10^{-14}\text{m}^{-2/3}$ 下随着传输距离的增加快速下降,当光束传输到远场时,探测概率曲线下降趋势减缓。图5(b)中:当 $C_n^2=1\times 10^{-16}\text{m}^{-2/3}$

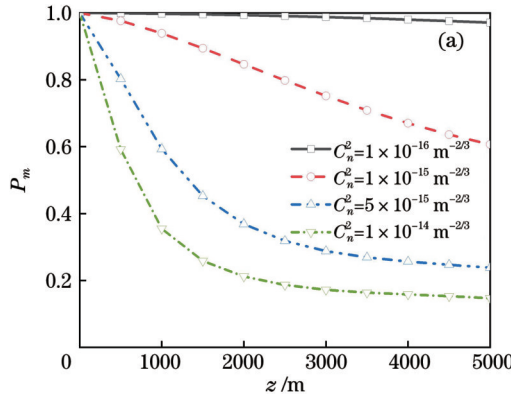


图5 不同近地面折射率结构常数下探测概率 P_m 和串扰概率 $P_{\Delta m}$ 随传输距离的变化。(a)探测概率 P_m ;(b)串扰概率 $P_{\Delta m}$
Fig. 5 Variations of detection probability P_m and crosstalk probability $P_{\Delta m}$ with transmission distance under different near-ground refractive index structure constants. (a) Detection probability P_m ; (b) crosstalk probability $P_{\Delta m}$

PVB光束的探测概率 P_m 与串扰概率 $P_{\Delta m}$ 受光束半径 r_t 的影响如图6所示。从图6(a)可以看出,当传输距离一定时,随光束半径 r_t 的增加,探测概率逐渐减

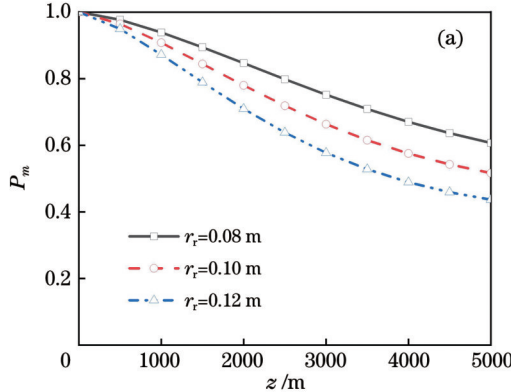
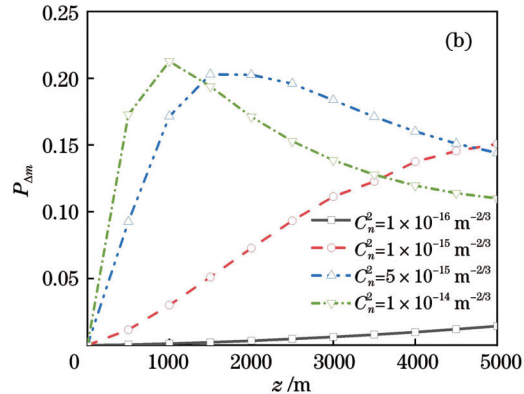


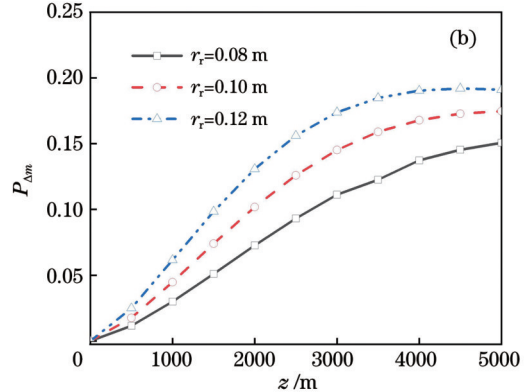
图6 不同光束半径下探测概率 P_m 和串扰概率 $P_{\Delta m}$ 随传输距离的变化。(a)探测概率 P_m ;(b)串扰概率 $P_{\Delta m}$
Fig. 6 Variations of detection probability P_m and crosstalk probability $P_{\Delta m}$ with transmission distance under different beam radii. (a) Detection probability P_m ; (b) crosstalk probability $P_{\Delta m}$

图7所示为不同non-Kolmogorov湍流系数 α 对PVB探测概率 P_m 以及串扰概率 $P_{\Delta m}$ 的影响。图7(a)中,当 α 接近3时, P_m 随着传输距离的增加而保持恒定,但如果 α 趋向于4,则探测概率 P_m 明显减小。当传输距离一定时,接收平面中的 α 越小, P_m 越大,原因是:当 α 接近3时,空间相干半径 ρ_0 接近无穷大^[23,26],湍流概率谱消失,从而使光束获得较高的探测概率 P_m ;当 α 接近4时,波前会出现纯倾斜^[23,26],在湍流大气传输中,倾斜会使光束偏离传输轴,探测概率 P_m 在 α 接近4的过程中逐渐减小。图7(b)中,当传输距离一定时,在 α

$10^{-16}\text{m}^{-2/3}$ 时,串扰概率 $P_{\Delta m}$ 几乎为0;当 $C_n^2=1\times 10^{-15}\text{m}^{-2/3}$ 时,串扰概率 $P_{\Delta m}$ 随着传输距离的增加而增大;当 $C_n^2=5\times 10^{-15}\text{m}^{-2/3}$ 和 $C_n^2=1\times 10^{-14}\text{m}^{-2/3}$ 时,串扰概率曲线有一个明显的特征,即先随传输距离增加到最大值后缓慢减弱。原因是:当近地面折射率结构常数较大时,不同OAM模态的能量占比被重新分配,导致更多的OAM模态链路中产生了明显的串扰。



小,螺旋谱的扩展程度增大。从图6(b)可以看出,当 $\Delta m=1$ 时,随着光束半径 r_t 的增加,其串扰概率 $P_{\Delta m}$ 增大。



从3.07增大到3.67的过程中,光束的串扰概率 $P_{\Delta m}$ 迅速增大。当 $\alpha=3.97$ 时,光束传输距离为2000 m的串扰概率 $P_{\Delta m}$ 达到最大值,随后开始缓慢减小,但此时光束出现较大的倾斜,由于受到孔径的限制,传输距离较大时,倾斜光束的主要能量已经不在接受孔径内,此时的概率已没有参考意义。

4 结 论

理论推导了PVB在non-Kolmogorov湍流下的螺旋相位谱解析表达式,建立了OAM模态探测概率和

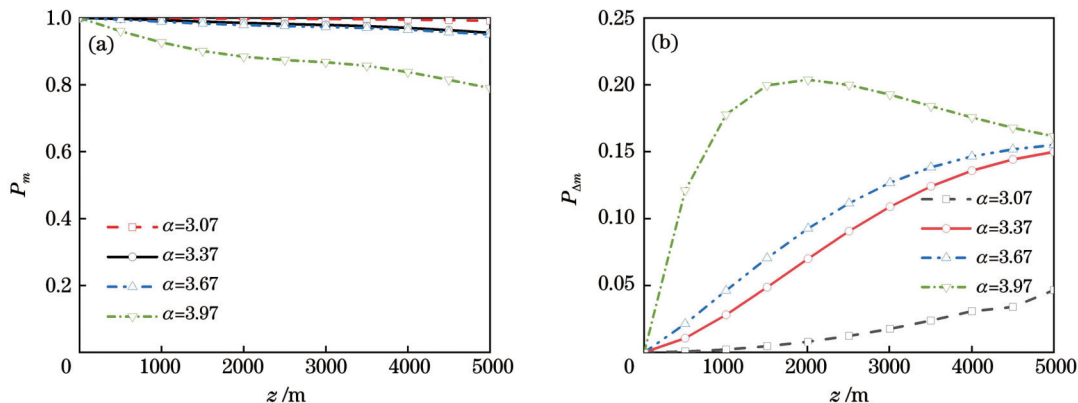


图7 不同湍流系数下探测概率 P_m 和串扰概率 $P_{\Delta m}$ 随传输距离的变化。(a)探测概率 P_m ; (b)串扰概率 $P_{\Delta m}$

Fig. 7 Variations of detection probability P_m and crosstalk probability $P_{\Delta m}$ with transmission distance under different turbulence parameters. (a) Detection probability P_m , (b) crosstalk probability $P_{\Delta m}$

串扰概率的理论模型。结果表明：大气湍流明显造成了PVB的螺旋相位谱扩展。PVB在近场的探测概率几乎不随发射处OAM模态变化，但当光束传输到远场时，探测概率随发射处OAM模态变化明显。并且，PVB的传输距离越大，大气湍流带来的负面影响越严重，随着远场发射处OAM模态、光束半径、近地面折射率结构常数和湍流系数的增大，经大气湍流传输后的探测概率下降。随着光束波长的增加，经大气湍流传输后PVB的探测概率增大。这些结果可为自由空间光通信中PVB的应用提供一定的参考。

参 考 文 献

- [1] 李新忠, 孟莹, 李贺贺, 等. 完美涡旋光束的产生及其空间自由调控技术[J]. 光学学报, 2016, 36(10): 1026018.
Li X Z, Meng Y, Li H H, et al. Generation of perfect vortex beams and space free-control technology[J]. Acta Optica Sinica, 2016, 36(10): 1026018.
- [2] Matsumoto N, Ando T, Inoue T, et al. Generation of high-quality higher-order Laguerre-Gaussian beams using liquid-crystal-on-silicon spatial light modulators[J]. Journal of the Optical Society of America. A, Optics, Image Science, and Vision, 2008, 25(7): 1642-1651.
- [3] Cang J, Xiu P, Liu X. Propagation of Laguerre-Gaussian and Bessel-Gaussian Schell-model beams through paraxial optical systems in turbulent atmosphere[J]. Optics & Laser Technology, 2013, 54: 35-41.
- [4] 刘会龙, 胡总华, 夏菁, 等. 无衍射光束的产生及其应用[J]. 物理学报, 2018, 67(21): 214204.
Liu H L, Hu Z H, Xia J, et al. Generation and applications of non-diffraction beam[J]. Acta Physica Sinica, 2018, 67(21): 214204.
- [5] Wei X L, Liu C M, Niu L T, et al. Generation of arbitrary order Bessel beams via 3D printed axicons at the terahertz frequency range[J]. Applied Optics, 2015, 54(36): 10641-10649.
- [6] 余京京, 任姣姣, 张丹丹, 等. 双锥面轴棱锥生长无衍射距离的太赫兹贝塞尔光束[J]. 光学学报, 2023, 43(7): 0726001.
Yu J J, Ren J J, Zhang D D, et al. Terahertz Bessel beams with long non-diffracting distance generated by biconical axicon[J]. Acta Optica Sinica, 2023, 43(7): 0726001.
- [7] Ostrovsky A S, Rickenstorff-Parrao C, Arrizón V. Generation of the “perfect” optical vortex using a liquid-crystal spatial light modulator[J]. Optics Letters, 2013, 38(4): 534-536.
- [8] Yan Y, Yue Y, Huang H, et al. Efficient generation and multiplexing of optical orbital angular momentum modes in a ring fiber by using multiple coherent inputs[J]. Optics Letters, 2012, 37(17): 3645-3647.
- [9] Ma H X, Li X Z, Tai Y P, et al. Generation of circular optical vortex array[J]. Annalen Der Physik, 2017, 529(12): 1700285.
- [10] Willner A E. Vector-mode multiplexing brings an additional approach for capacity growth in optical fibers[J]. Light: Science & Applications, 2018, 7(3): 18002.
- [11] Wang J A. Advances in communications using optical vortices [J]. Photonics Research, 2016, 4(5): B14-B28.
- [12] Zhou H L, Dong J J, Shi L, et al. Hybrid coding method of multiple orbital angular momentum states based on the inherent orthogonality[J]. Optics Letters, 2014, 39(4): 731-734.
- [13] Zhang Y X, Wang Y G, Xu J C, et al. Orbital angular momentum crosstalk of single photons propagation in a slant non-Kolmogorov turbulence channel[J]. Optics Communications, 2011, 284(5): 1132-1138.
- [14] Zhang Y X, Cang J. Effects of turbulent aberrations on probability distribution of orbital angular momentum for optical communication[J]. Chinese Physics Letters, 2009, 26(7): 074220.
- [15] Aksenen V P, Kolosov V V, Filimonov G A, et al. Orbital angular momentum of a laser beam in a turbulent medium: preservation of the average value and variance of fluctuations[J]. Journal of Optics, 2016, 18(5): 054013.
- [16] Yang C Y, Lan Y, Jiang X Y, et al. Beam-holding property analysis of the perfect optical vortex beam transmitting in atmospheric turbulence[J]. Optics Communications, 2020, 472: 125879.
- [17] 黎芳, 唐华, 江月松, 等. 拉盖尔-高斯光束在湍流大气中的螺旋谱特性[J]. 物理学报, 2011, 60(1): 014204.
Li F, Tang H, Jiang Y S, et al. Spiral spectrum of Laguerre-Gaussian beams propagating in turbulent atmosphere[J]. Acta Physica Sinica, 2011, 60(1): 014204.
- [18] Zhu Y, Zhang L C, Hu Z D, et al. Effects of non-Kolmogorov turbulence on the spiral spectrum of Hypergeometric-Gaussian laser beams[J]. Optics Express, 2015, 23(7): 9137-9146.
- [19] Liu Z, Wei H Y, Cai D M, et al. Spiral spectrum of Laguerre-Gaussian beams in slant non-Kolmogorov atmospheric turbulence [J]. Optik, 2017, 142: 103-108.
- [20] Wang Y K, Bai L, Xie J Y, et al. Spiral spectrum of high-order elliptic Gaussian vortex beams in a non-Kolmogorov turbulent atmosphere[J]. Optics Express, 2021, 29(11): 16056-16072.
- [21] Vaity P, Rusch L. Perfect vortex beam: Fourier transformation of a Bessel beam[J]. Optics Letters, 2015, 40(4): 597-600.
- [22] Wang H Y, Yang Z H, Liu L, et al. Orbital angular momentum spectra of twisted Laguerre-Gaussian Schell-model beams

- propagating in weak-to-strong Kolmogorov atmospheric turbulence[J]. Optics Express, 2023, 31(2): 916-928.
- [23] Rao C H, Jiang W H, Ling N. Spatial and temporal characterization of phase fluctuations in non-Kolmogorov atmospheric turbulence[J]. Journal of Modern Optics, 2000, 47 (6): 1111-1126.
- [24] Pinnell J, Rodríguez-Fajardo V, Forbes A. How perfect are perfect vortex beams?[J]. Optics Letters, 2019, 44(22): 5614-5617.
- [25] 陈鸣, 高太长, 刘磊, 等. 非Kolmogorov湍流相位屏仿真及对光束传输模拟的影响[J]. 强激光与粒子束, 2017, 29(9): 43-51. Chen M, Gao T C, Liu L, et al. Influence of non-Kolmogorov turbulence phase screen based on equivalent structure constant on beam quality in transmission[J]. High Power Laser and Particle Beams, 2017, 29(9): 43-51.
- [26] Stribling B E, Welsh B M, Roggemann M C. Optical propagation in non-Kolmogorov atmospheric turbulence[J]. Proceedings of SPIE, 1995, 2471: 181-196.

Spiral Phase Spectra of Perfect Vortex Beams Transmitting Through Atmospheric Turbulence

Li Siyao, Ding Zhoulin, Hou Chunyu, Wang Weijun, Ma Jiaxin, Yu Yongji*

Jilin Key Laboratory of Solid Laser Technology and Application, School of Physics, Changchun University of Science and Technology, Changchun 130022, Jilin, China

Abstract

Objective Vortex beam is a beam that carries orbital angular momentum (OAM). The perfect vortex beam (PVB) is a new type of beam that has emerged in recent years. Compared with other traditional vortex beams, the PVB has the property that the radius of the optical ring does not increase with the increase in OAM mode, which has attracted much attention in the field of free-space optical communication. Moreover, the different OAM modes of the vortex beam are orthogonal to each other and can be used to expand the channel capacity of optical communication systems. The OAM dimension of the vortex beam can also be used for signal coding, and since the number of modes of OAM modes is not limited (it can be any integer), it is theoretically possible to carry an infinite amount of bits of information in a single code element. However, vortex beam transmission in the atmosphere will be affected by atmospheric turbulence and produce distortion, and atmospheric turbulence makes its light intensity distribution uneven. Spiral phase distortion can result in the expansion of the spiral spectrum, cause crosstalk between different modes of the vortex beam, and reduce the signal-to-noise ratio of the communication system, thus leading to the degradation of the communication quality in practical applications. In this study, based on the Rytov approximation, the analytical expression of the spiral phase spectrum of the PVB at the receiving aperture is derived, and the probability of detection and crosstalk probabilistic models of the OAM mode of the PVB is established. The effects of different parameters on the PVB in a turbulent atmosphere are analyzed in the context of the light intensity distribution characteristics of the PVB in free space transmission. These results are expected to provide a reference for the application of PVB in free-space optical communication.

Methods In this paper, an analytical expression for the spiral phase spectrum of the PVB is derived theoretically. First, the complex amplitudes of PVBs transmitted in atmospheric turbulence in the weakly turbulent region are obtained using the Rytov approximation based on the optical field distribution of PVBs in the source plane and in free space. Then, in order to describe the OAM mode of the PVB more clearly, the expression of the vortex beam is decomposed into the form of a spiral harmonic function. After that, the non-Kolmogorov probability spectrum is used to describe the effect of atmospheric turbulence on the OAM of the PVB. Then, by using the quadratic approximation of the wave structure function, the analytical expression of the OAM mode probability density of the PVB is obtained. In the next step, the spiral phase spectrum is defined, and the detection probability and the crosstalk probability of the OAM mode of the PVB are modeled. In addition, the effect of each beam element on the beam transmission in atmospheric turbulence and the light intensity characteristics of PVB transmission are analyzed using MATLAB software.

Results and Discussions The PVB has the property that the radius of the beam does not increase with the increase in the OAM mode. As the OAM mode at the transmitter changes, the detection probability and crosstalk probability curves corresponding to different initial OAM modes at the transmitter almost coincide when transmitting to the near field, and the difference between the detection probability and crosstalk probability curves corresponding to different initial OAM modes at the transmitter increases significantly when transmitting to the far field (Fig. 3). In addition, when the beam is

transmitted to the far field, and the quantum number difference is 1, larger OAM mode at the emission indicates higher crosstalk probability. The crosstalk probability occurs mainly between two neighboring OAM states (Fig. 3). Furthermore, the variation of PVB light intensity with distance in atmospheric turbulence can reveal the evolution of the PVB light field (Fig. 4). In addition, the crosstalk probability curve of PVB has a significant feature in the state with a large refractive index structure constant near the ground: it first increases to a maximum with the transmission distance and then slowly decreases (Fig. 5).

Conclusions In this paper, an analytical expression for the spiral phase spectrum of a PVB under non-Kolmogorov turbulence is derived theoretically. Theoretical models of OAM modal detection probability and crosstalk probability are developed. The results show that the atmospheric turbulence significantly causes the spiral phase spectrum expansion of the PVB. The detection probability curve of the PVB in the near field hardly varies with the OAM mode at the transmitter, while it varies significantly with the OAM mode at the transmitter when the beam is transmitted to the far field. This is because the PVB transmitted to the far field becomes a Bessel-like beam, and its beam radius varies significantly with the OAM mode at the transmitter. Moreover, a long transmission distance of the PVB beam indicates a more severe negative impact of atmospheric turbulence. The detection probability of the beam after atmospheric turbulent transport decreases as the number of OAM modes at the transmitter, beam radius, refractive index structure constant near the ground, and turbulence coefficient increase. As the beam wavelength increases, the detection probability of the PVB after atmospheric turbulent transport increases. These results provide a certain reference value for the implementation of PVBs in atmospheric turbulence for optical communication links in free space.

Key words atmospheric optics; perfect vortex beam; orbital angular momentum; turbulent atmosphere; spiral phase spectra